

Enhanced Methanol Oxidation on Nanoporous Nickel Phosphate Modified Platinum Electrode in Alkaline Solution

Ahmed. H. Touny^{1,3,*}, Mahmoud. M. Saleh^{1,2,*}

¹ Department of Chemistry, College of Science, King Faisal University, Al-Hassa, Saudi Arabia

² Department of Chemistry, Faculty of Science, Cairo University, Cairo, Egypt

³ Department of Chemistry, Faculty of Science, Helwan University, Helwan, Egypt

*E-mail: aahamed@kfu.edu.sa, atouny@yahoo.com, mmsaleh@kfu.edu.sa
mahmoudsaleh90@yahoo.com

Received: 26 July 2017 / Accepted: 11 October 2017 / Published: 16 December 2017

The theme of this paper is to enhance the methanol oxidation via nanoporous nickel phosphate (nano-NiPh) modified platinum (Pt) electrode in alkaline solution. Nickel phosphate material is synthesized by a simple reflux-based method and characterized by Scanning electron Microscope (SEM), tunneling electron microscopy (TEM), FT-IR absorption spectroscopy and X-ray diffraction (XRD). The NiPh has the chemical structure of $\text{Ni}_3(\text{PO}_4)_2 \cdot 8\text{H}_2\text{O}$ with nanoporous features and monoclinic crystallographic form. Nickel phosphate particles produced in agglomerated particles with a crystal growth along one direction (c-direction) to form rods or whisker-shape structures. The surface of the rods formed with nanoporous structure (pore diameter ~ 30 nm). These pores are distributed throughout the surface of the NiPh particles. Platinum modified with nano-NiPh (nano-NiPh/Pt) demonstrates enhanced methanol oxidation from alkaline solution. The peak of direct current (forward sweep), the onset potential and the ratio of the direct to indirect currents have demonstrated the enhancement of the MeOH oxidation at the nano-NiPh/Pt compared to that obtained with unmodified Pt electrode.

Keywords: Methanol, Pt, Nickel phosphate, fuel cell, nanoporous

1. INTRODUCTION

Direct methanol fuel cell (DMFC) represents an important category of FC since they have high power and are considered to be safe (methanol being a liquid fuel) compared to H_2 /air FC. Platinum and Pt-based electrocatalysts have been usually used as anodes in such DMFC [1-3]. However, platinum electrodes are suffering from poisons, limited sources and also they are costly [4]. To decrease those drawbacks, Pt electrode was modified with different metals [5,6], metal oxides [7,8]

and carbon nanotubes [9]. This can improve the performance of the Pt-based electrodes towards the electrochemical oxidation of methanol. Such co-catalyst provides an enhancement of the MeOH oxidation by facilitating the oxidation of the poisoning carboneous intermediates (*e.g.*, CO). Based on the literatures, there is no any report about metal salts such as metal phosphate as a co- catalyst for enhancement of the electrocatalytic oxidation of methanol on Pt electrodes. Nickel phosphate (NiPh) has been found in several applications. Particularly, it has been used as supercapacitors [10,11], lithium batteries [12,13], catalytic reactions [14] and electrocatalytic reactions [15]. According to the literatures, NiPh has been currently prepared via different approaches such as wet chemical process [16], hydrothermal [17], solvothermal [18] and sol-gel technique [19]. Those different approaches led to a variation in the chemical composition, and structural and morphological properties that considered primary reasons for the presence of NiPh in several applications. To the best of our knowledge, the influence of modifying Pt electrode with nanoporous NiPh particles produced by reflux technique on the electrocatalysis of methanol has not been reported. So the main objective of this paper is to modify the surface of the platinum with NiPh which will be fabricated by reflux method.

2. EXPERIMENTAL

2.1. Electrode Fabrication

Synthesis of NiPh via a reflux-based route was previously prescribed [20]. Generally a reagent grade of nickel nitrate ($\text{Ni}(\text{NO}_3)_2 \cdot 6\text{H}_2\text{O}$) was mixed with ammonium dibasic phosphate ($(\text{NH}_4)_2\text{HPO}_4$) to produce a precipitate of nickel phosphate. Initially a 5 ml of 2 M of nickel nitrate solution was added to a 5 ml of dibasic ammonium hydrogen phosphate (2 M) at room temperature in a round bottom flask with continuous stirring. 3-4 drops of conc. nitric acid were added to dissolve the produced precipitate and to obtain a uniform homogenous solution. A 50 ml of 0.3 M urea solution was inserted into the formed homogenous solution. The homogeneous solution was thermostatted and refluxed at a fixed refluxing temperature of 90 °C with a consistent stirring for 18 h. The formed suspension was left to cool to room temperature, filtered and washed several times with bi-distilled water. Lastly, the prepared precipitate was dried in an oven at 100 °C for overnight. The catalyst ink of NiPh, for being anchored on the surface of Pt, was prepared by adding (2.5 mg) of NiPh powder to a solution containing 2.5 ml isopropanol and 50 μL of Nafion solution (5% in water) and sonicated for 30 min in an ice bath.

Pt electrode ($d = 2$ mm) is used here as the underlying substrate for NiPh. Initially the electrode was precisely cleaned using by mechanical polishing then followed by potential cycling in 0.25 M H_2SO_4 until The CV characteristics of the Pt were obtained. Next, 50 μL of a freshly prepared NiPh suspension (prepared as given above) is casted onto the thus cleaned Pt electrode and left overnight to dry in room temperature. The prepared loading level is 1.0 mg cm^{-2} (of the electrode surface area).

2.2 Measurements

The phase assemblage of the as-synthesized samples was studied using X-ray diffraction (XRD). The XRD analysis was performed using a diffractometer ((PANalytical, X'Pert PRO) equipped with a Cu K α radiation ($\lambda = 1.5406 \text{ \AA}$). XRD radiation generated at 40 KV and a current of 44 mA with a scan rate of $2^\circ/\text{min}$ over a 2° range of $4\text{--}80^\circ$. The infrared spectra (FT-IR) was performed by using JASCO 3600 spectrophotometer using ca. 0.5 mm KBr pellets containing 2.5 wt% sample. High resolution transmission electron micrograph (TEM, JEOL-JEM-1230) at an accelerating voltage of 200 kV was used. The surface morphology of the as-prepared NiPh samples was observed using scanning electronic microscopy (SEM, Model JEOL JSM 5410, Japan) at an accelerating voltage of 5KV. The BET analysis of the NiPh sample was measured using a Micrometrics ASAP2010 volumetric adsorption apparatus. Electrochemical measurements were performed using Gamry potentiostat/galvanostat supported with Gamry electrochemical analysis technique. Electrochemical measurements were carried out in a conventional three-electrode cell. The counter electrode was made of a platinum coil. The reference electrode was Ag/AgCl/KCl (sat.) with a Luggin probe positioned near the electrode surface. The potential throughout the text is referred to the above reference electrode. The measurements were repeated to test the reproducibility of the results.

3. RESULTS AND DISCUSSION

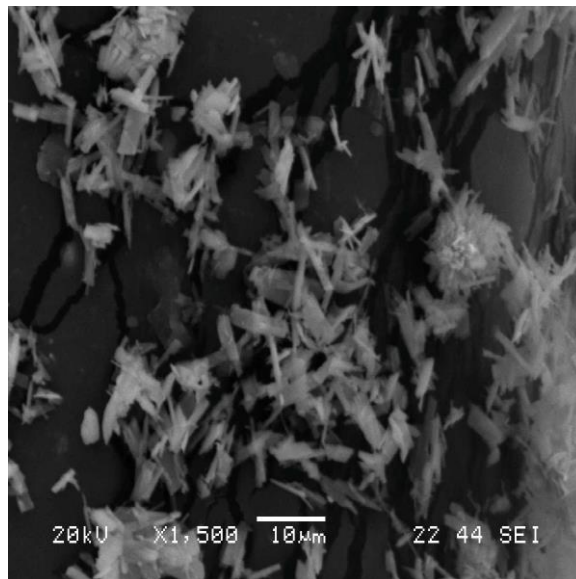


Figure 1. SEM of NiPh synthesized by the method discussed in the experimental section

The SEM micrographical structure of the NiPh powder is shown in Fig. 1. Qualitatively, it can be seen that the nickel phosphate particles produced in agglomerated particles with a crystal growth along one direction (c-direction) to form rods or whisker-shape structures. The average size of the nanoparticles is close to $150 \text{ nm} \times 800 \text{ nm}$. It may possibly to conclude that these nanoparticles formulations have almost uniform size distributions with different orientations.

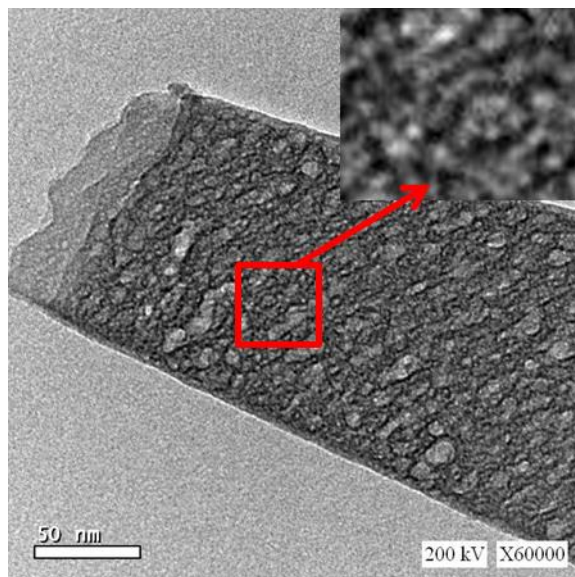


Figure 2. TEM of NiPh. Inset shows magnification of surface porous structure

Figure 2 shows the typical TEM (high magnification) image of the NiPh used in this investigation. The analysis of the TEM image indicates that the NiPh particles have been formed with a relatively uniform rod morphological structure. Additionally, the analysis shows that the surface of the rods formed with nanoporous structure (pore diameter ~ 30 nm). These pores are distributed throughout the surface of the NiPh particles. These nanoporous surfaces can significantly facilitate the ion transportation and consequently enhance the performance of these materials in electrochemical uses [21].

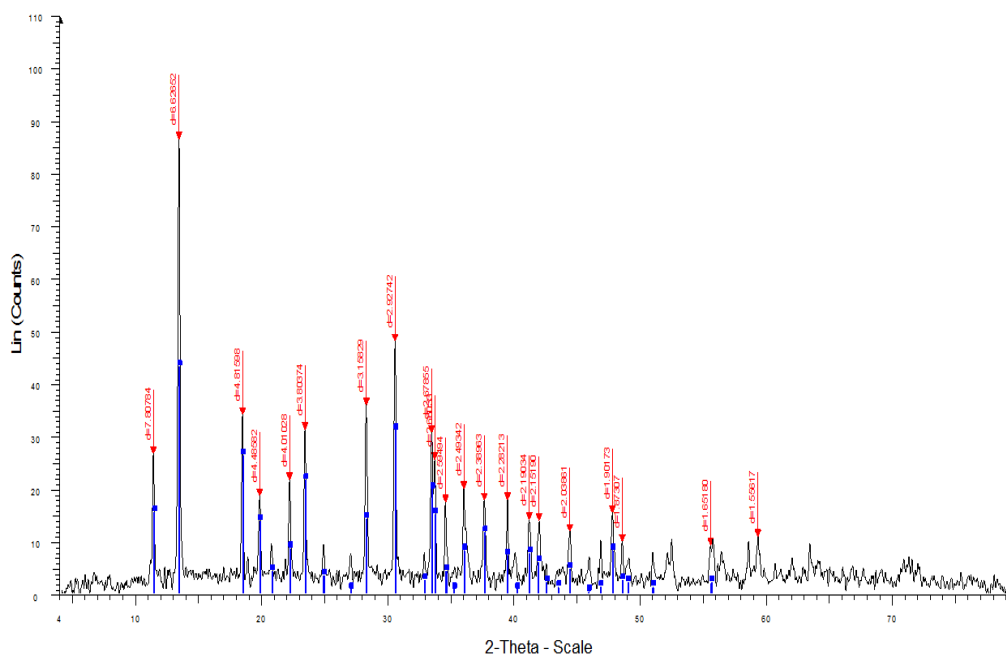


Figure 3. XRD pattern of NiPh.

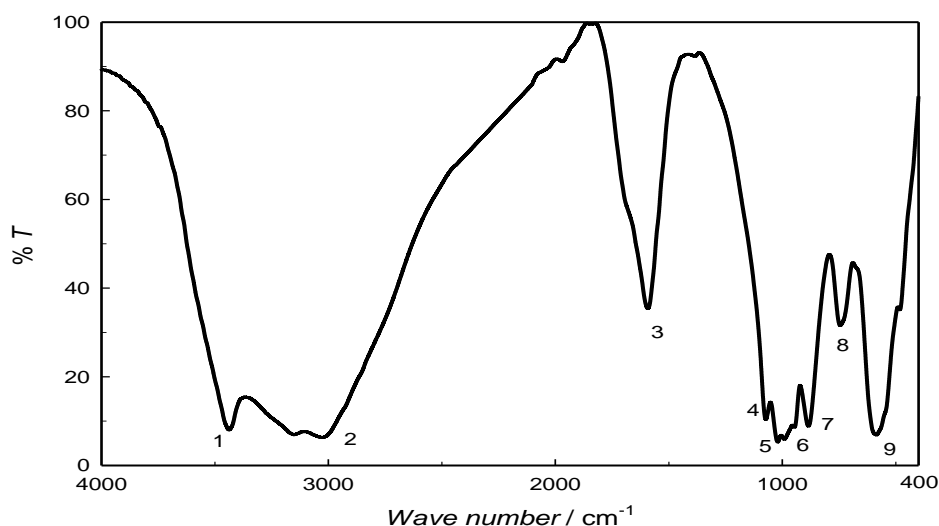
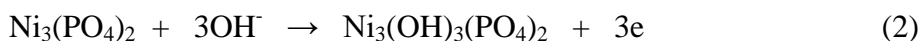


Figure 4. FT-IR spectrum of NiPh.

The XRD pattern shown in Fig. 3 examines the crystallinity and purity of the NiPh powder. It should be noted that the XRD pattern consists of sets of peaks which correspond to the NiPh particles. Those peaks are indexed to the monoclinic crystalline structure of $\text{Ni}_3(\text{PO}_4)_2 \cdot 8\text{H}_2\text{O}$ in accordance with that of the standard spectrum (PDF No. 33-0951) [22]. The XRD pattern shows that the samples are formed with a single phase structure. The average grain size, D_{hkl} is estimated by means of the Scherrer formula [23]. The average value D_{hkl} is estimated to be 51.0 nm for the NiPh prepared by the present experimental conditions. Using the BET analysis, the NiPh specific surface area was found to be 22.3 m^2/g . The average pore size was 12.3 nm.

The FT-IR spectra for the NiPh powder is shown in Fig 4. The spectrum reveals that there are three vibrational broad bands in the range of 3000–3450 cm^{-1} (from 1 to 2 peaks) assigned to the OH stretching vibration of the H_2O and they are validated by XRD (*c.f.* Fig. 3). The bending vibrational mode of water molecules appear at 1592 cm^{-1} (peak 3) [24, 25] and the band assigned at 740 cm^{-1} (peak 8) is attributed to the librational modes of water molecule. Based on literature those bands were disappeared when the nickel phosphate powdered materials were calcined at higher temperature [26]. The vibrational bands of the PO_4^{3-} anion are observed around 1072, 1022, 991 and 883 cm^{-1} (peaks 4, 5, 6 and 7) [24,25]. Those bands are corresponding to the tetrahedral stretching vibrations and the strong band found at $\sim 580 \text{ cm}^{-1}$ (peak 9) is assigned to P-O vibrations.

The cyclic voltammogram (CV) responses for the unmodified Pt (a) and modified Pt with nano-NiPh (nano-NiPh/Pt) (b) in 0.25 M KOH with a scan rate of 100 mV s^{-1} are shown in Fig 5. The Pt has its typical peaks in the KOH electrolyte. The peaks for Pt in the potential range from -0.4 to -0.8 V and at -0.12 V assigned for the H-absorption/desorption and Pt-oxide reduction, respectively. In case of modified electrode, another redox peak appears in the range of 0.5-0.6 V which can be assigned to the redox couple Ni(II)/Ni(III) according Eq. 2; [27]



The above redox couple appears in Fig. 5 and Eq. 2 was done by invasion of the OH⁻ ions using potential cycling of the nano-NiPh/Pt electrode in 0.25 M KOH (blank) for about 50 cycles. During those cycles the redox peaks emerged and the peak current of the cathodic and anodic peaks increases until it reaches constant values at cycle number ~ 50. The peaks appearing in Fig. 5 for the Ni(II)/Ni(III) couple were recorded after finishing from the potential cycling process. This is in accordance with our previously published work [20]. The appearance of the characterized peaks of Pt in the presence of its surface modification by nano-NiPh implies that the Pt electrode is not fully covered with those nanoparticles. The difference in the peak height of the Pt-oxide reduction on both electrodes in Fig. 5 can be used to estimate the surface coverage of the Pt with NiPh.

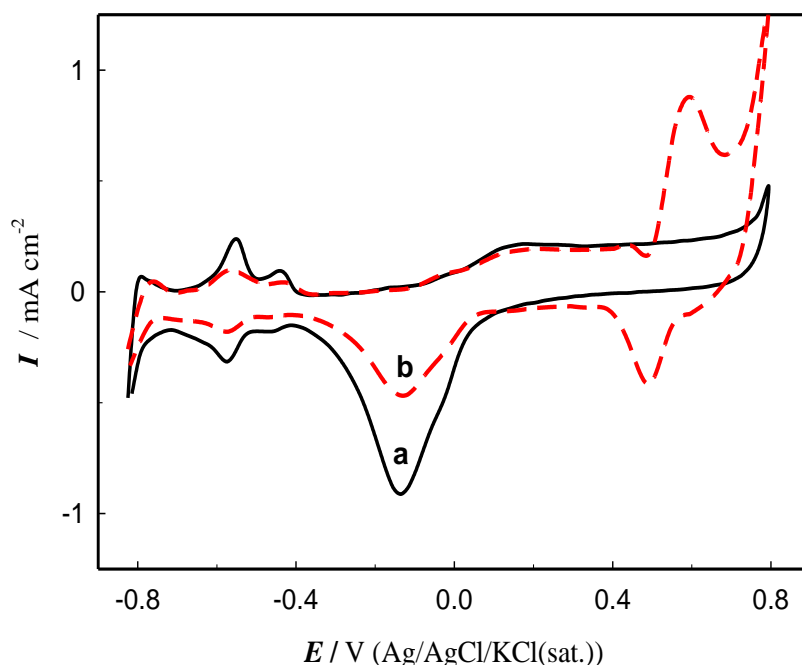


Figure 5. CV responses in blank 0.25 M KOH at scan rate of 100 mV s⁻¹; a) Pt and b) nano-NiPh/Pt.

The electrochemical active surface area of the bare Pt and modified Pt (nano-NiPh/Pt) electrodes can be estimated from the charge associated with the surface reduction of Pt oxide. This can be done assuming 420 $\mu\text{A cm}^{-2}$ (of the electrochemical active surface area) for Pt-oxide reduction [28]. The electrochemical active surface area was estimated to be 0.164 and 0.092 cm² for bare Pt and nano-NiPh/Pt, respectively. The surface coverage can be estimate from the relation; $\theta = 1 - (A_{\text{NiPh}}/A_{\text{bare}})$, where A_{NiPh} and A_{bare} is the surface area of the modified Pt electrode (nano-NiPh/Pt) and the bare (unmodified) Pt electrode, respectively. Accordingly, the surface coverage of the Pt surface was estimated to be 0.42.

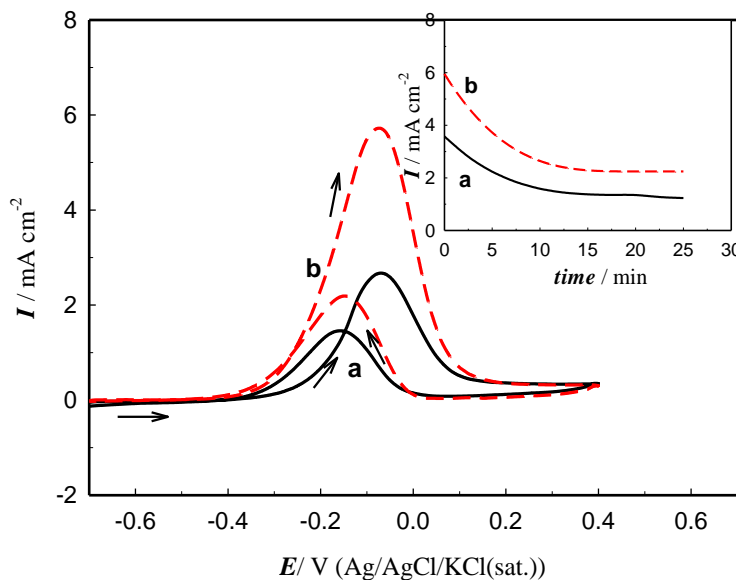


Figure 6. CV responses (inset chronoamperometric curves) in 0.25 M KOH + 0.25 M MeOH; a) Pt and b) nano-NiPh/Pt.

In this investigation, the electrochemical activity of the manufactured nano-NiPh/Pt towards methanol oxidation was examined in Fig 6. The CV responses of the unmodified Pt (a) and modified nano-NiPh/Pt (b) in 0.25 M KOH containing 0.25 M MeOH at scan rate of 100 mV s^{-1} are shown in Fig. 6. The figure demonstrates some important features. In case of unmodified Pt electrode the two oxidation peaks appear at -0.07 and -0.15 V for the forward and reverse sweeps, respectively. While for modified Pt the two peaks occur at -0.08 and -0.15 V for the forward and reverse sweeps, respectively. The onset potential of MeOH oxidation ($I = 0.1 \text{ mA cm}^{-2}$) is -0.25 V and -0.32 V for Pt and nano-NiPh/Pt, respectively. The peak current of MeOH oxidation at nano-NiPh/Pt is more than the double of that at the bare Pt electrode. For instance, I_p is 2.5 and 5.8 mA cm^{-2} for Pt and nano-NiPh/Pt, respectively. The ratio of the direct (forward sweep) to the indirect (reverse) peak currents at nano-NiPh/Pt is higher than that at the bare Pt electrode (2.7 and 1.7 , respectively). The chronoamperometry curves shown in the inset of the figure demonstrates the long-term activity of the nano-NiPh/Pt compared to the bare Pt electrode. The above results demonstrate that the nano-NiPh/Pt is more efficient in MeOH electrooxidation than the unmodified Pt electrode. The role of the OH^- ions has a crucial role in diminishing the poisoning of the Pt surface with the carbonaceous products of the MeOH oxidation. The above enhancement of the MeOH oxidation can be attributed to the bi-functional mechanism. The above mechanism involves the adsorptive action of O-type species on the NiPh moieties at lower potential and hence promotes the oxidation of CO to CO_2 via surface reaction between O-type species (e.g., $-\text{OH}$) and adsorbed carbonaceous species i.e., CO_{ads} . Various types of co-catalysts that can offer the bifunctional mechanism. These include metals (e.g., Ni, Co, Pd) and metal oxides (e.g., RuO, CeO_2 , V_2O_5 and NiO) [29-35]. In this context NiPh in the present work offers this job as it is obvious from our work. This can be supplied by the NiPh co-catalyst with the Pt surface in a common strategy of bifunctional role of the NiPh. This can facilitate the oxidation of the intermediate products to gaseous CO_2 and hence liberate more Pt active sites for MeOH oxidation. The

synergism of the MeOH oxidation may take place according to the possible mechanism given below; [36]



The NiPh may enhance the tolerance of the Pt surface to CO poisonous by formation of the OH_{ads} moieties at lower potential on the catalyst surface which in turn can react with the CO-like species to produce CO_2 and hence releasing the free Pt active sites required for the MeOH oxidation.

4. CONCLUSIONS

Nanoporous nickel phosphate has been synthesized by a reflux method and used as a co-catalyst with Pt for MeOH electrochemical oxidation in alkaline solution. The structural and morphological characteristics of the nano-NiPh were studied by different techniques. The nano-NiPh/Pt demonstrated much higher performance for MeOH oxidation than that of bare Pt electrode.

ACKNOWLEDGEMENT

This work was supported by the grants from the Deanship of Scientific Research, King Faisal University (project # 170054). The financial contribution is gratefully acknowledged. The authors also thank the Department of Chemistry, College of Science, King Faisal University for getting this article published.

References

1. S. Q. Song, W.J. Zhou, Z.H. Zhou, L.H. Jiang, G.Q. Sun, Q. Xina, V. Leontidis, S. Kontou, P. Tsiakarasc, *Int. J. Hydrogen Energy*, 30 (2005) 995.
2. L. Zhao, S. Cu-Lei, L. Jia-Liong, Z. Jing-Jia, Z. Li-Mei, and W. Zhen-Bo, *Catalysis Communications*, 86 (2016) 46.
3. S. K. Hassaninejad-Darzi, *J. Electroceramics*, 33 (2014) 252.
4. Y. Feng, L. Bi, Z. Liu, D. Kong, and Z. Yu, *J. Catalysis*, 290 (2012) 18.
5. Q. Jiang, L. Jiang, S. Wang, J. Qi, and G. Sun, *Catalysis Communications*, 12 (2010) 67.
6. M. M. Tusi, N. S.O. Polanco, S. G. da Silva, E. V. Spinacé, and A. O. Neto, *Electrochem. Communications*, 13 (2011) 143.
7. W. Huang et al., *Nat. Commun.*, 6 (2015)10035
8. C. Xu, R. Zeng, P. K. Shen, and Z. Wei, *Electrochim. Acta*, 51 (2005) 1031.
9. Z. Liu, B. Zhao, C. Guo, Y. Sun, Y. Shi, H. Yang, and Z. Li, *J. Colloid Interface Science*, 351 (2010) 233 .
10. J. Zhao, H. Pang, J. Deng, Y. Ma, Bo Yan, X. Li, S. Li, J. Chen, and W. Wang, *Cryst. Eng. Comm.*, 15 (2013) 5950.
11. J. Yang, J. Tan, and D. Ma, *J. Power Sources*, 260 (2014) 169.
12. C. V. Ramana, A. Ait-Salah, S. Utsunomiya, U. Becker, A. Mauger, F. Gendron, and C. M. Julien, *Chem. Mater.*, 18 (2006) 3788.
13. M. Minakshi, P. Singh, D. Appadoo, and D. E. Martin, *Electrochim. Acta*, 56 (2011) 4356.

14. Y. Zhan, M. Lu, S. Yang, Z. Liu, and J. Lee, *ChemElectroChem*, 3(4) (2016) 615.
15. Y. Li, and C. Zhao, *Chem. Mater.*, 28 (2016) 5659.
16. X. Wang, Q. Gao, C. Wu, J. Hu, and M. Ruan, *Microporous and Mesoporous Materials*, 85 (2005) 355.
17. H. Wu, Y. Gaob, and H. Li, *Cryst. Eng. Comm.*, 12 (2010) 3607.
18. G. Demazeau, *J. Mater Sci.*, 43 (2008) 2104.
19. J. Yu, A. Wang, J. Tan, X. Li, J. Bokhoven, and Y. Hu, *J. Materials Chem.*, 18 (2008) 3601.
20. M. A. Al-Omar, A.H. Touny, and M.M. Saleh, *J. Power Sources*, 342 (2017)1032.
21. Y. Zhang, and Z. Guo, *Materials Chemistry and Physics*, 171 (2016) 208.
22. J. V. Smith (Ed.), X-ray Powder Data File, American Society for Testing Materials, 1960.
23. I. Krishnan, A. Bhatia, and H. Varma, *Dental materials*, 32 (2016) 664.
24. S. Kullyakool, C. Danvirutai, K. Siri Wong, and P. Noisong, *J. Therm. Anal. Calorim*, 115 (2014) 1497.
25. P. Noisong, C. Danvirutai, T. Srithanratana, and B. Boonchom, *Solid State Sci.*, 10 (2008) 1598.
26. C. M. Burba, R. Frech, *Spectrochim. Acta*, 65(A) (2006) 44.
27. Y. Zhao, Z. Chen, D. B. Xiong, Y. Qiao, Y. Tang, and F. Gao, *Sci. Rep.*, 6(2016) 17613
28. S. Trasatti and O. A. Petrii, *Pure Appl. Chem.*, 63 (1991) 711.
29. E. Antolini, J. R.C. Salgado, and E. R. Gonzalez, *Appl. Catal. B: Environmental*, 63 (2006) 137.
30. C.W. Xu, R. Zeng, P.K. Shen, and Z.D. Wei, *Electrochim. Acta*, 51 (2005) 1031
31. P. Justin, and G.R. Rao, *Catal. Today*, 141 (2009) 138.
32. P.K. Shen, C.W. Xu, R. Zeng, and Y.L. Liu, *Electrochem. Solid-State Lett.*, 9 (2006) A39.
33. X. Zhang, F. Zhang, Re Guan, and K. Chan, *Mat. Res. Bulletin*, 42 (2007) 327.
34. E. E. Switzer, T. S. Olson, A. K. Datye, and P. Atanassov, M. R. Hibbs, C. J. Cornelius, *Electrochim. Acta*, 54 (2009) 989.
35. X. Zhang, K. Tsang, and K. Chan, *J. Electroanal. Chem.*, 573 (2004) 1.
36. A. Maksic, Z. Rakocevic, M. Smiljanic, M. Nenadovic, and S. Strbac, *J. Power Sources*, 273(2015) 724.

© 2018 The Authors. Published by ESG (www.electrochemsci.org). This article is an open access article distributed under the terms and conditions of the Creative Commons Attribution license (<http://creativecommons.org/licenses/by/4.0/>).